COMMUNICATIONS IN COMPUTATIONAL PHYSICS
Vol. **2**, No. 4, pp. 760-782

Commun. Comput. Phys.
August 2007

Numerical Method for Boltzmann Equation with Soroban-Grid CIP Method

Youichi Ogata, Hyo-Nam Im and Takashi Yabe*

Department of Mechanical Sciences and Engineering, Tokyo Institute of Technology, 2-12-1 Meguro-ku, Ookayama 152-8552, Japan.

Received 6 October 2006; Accepted (in revised version) 25 November 2006

Available online 29 January 2007

Abstract. A new numerical scheme to solve the Boltzmann equation in phase space for rarefied gas is described on the basis of the Cubic Interpolated Propagation (CIP) method. The CIP procedure is extended to adaptive unstructured grid system by the Soroban grid. The grid points in velocity space can move dynamically following the spread of velocity space in a spatially localized manner. Such adaptively moving points in velocity space are similar to the particle codes but can provide higher-order-accurate solutions. Numerical solutions obtained by the Soroban-grid CIP are examined and the validity is discussed.

PACS (2006): 02.70.-c, 47.11.-j, 47.45.-n

Key words: CIP, Boltzmann equation, Soroban grid.

1 Introduction

Various kinds of numerical methods have been used for the Boltzmann equation in application to plasma physics, hydrodynamics including rarefied gas, free molecules flow and so on. There are some characteristic phenomena in rarefied gas such as Knudsen layer [1], shock wave [2,3], Rayleigh problem [4]. Numerical methods for the Boltzmann equation can be roughly divided into two classes. One is called the Lagrangian methods. Among these Lagrangian schemes, one of the most popular particle methods is the Particle in cell (PIC) method [5]. This method has been considered to be quite stable even if only a few computational particles per one grid cell are used. However, this scheme essentially involves some disadvantages stemming from statistical numerical noise.

Another Lagrangian approach is the Monte Carlo method (DSMC:Direct Simulation with Monte-Calro method) [3,6]. It has been used for rarefied gas dynamics described by

*Corresponding author. *Email addresses:* yogata@mech.titech.ac.jp (Y. Ogata), leemhn@gmail.com (H.-N. Im), yabe@mech.titech.ac.jp (T. Yabe)

the Boltzmann equation. These Lagrange-based schemes are stable even with the small number of particles and they have been used for some simulations of hyper-dimensional Boltzmann-Vlasov equation. However, there is still a disadvantage that the computation cost in the Monte-Calro method is quite large for some flows like near continuum flows even though the drastic improvement of computer technology is making the computation much faster than ever before.

An alternative to the particle method or the Monte-Calro method is the Eulerian method that uses a hyper-dimensional computational mesh in phase space. There have been some simulations of the standard Boltzmann equations performed by finite difference method [7]. We here propose to use the Cubic Interpolated Propagation (CIP) method that was proposed by Yabe [8–10]. In the CIP scheme, first spatial derivatives are introduced as free parameters on each grid point and we do not have to solve matrix to make cubic-interpolation function even in multi-dimensional cases. Therefore, the time evolution of the derivatives as well as the function values are calculated from a model equation that is consistent with the master equation and the scheme becomes the third-order accuracy in time and space. One of the biggest advantages of the CIP method is that the phase error and amplification factor are better than those of the other conventional schemes with less number of grid points [11]. This implies that the CIP method has possibility to overcome some problems that are intrinsic in the particle method or the Monte-Calro method.

The CIP method has been successfully applied to various complex fluid flow problems of both compressible and incompressible flow, such as laser-induced evaporation, skimmer [12], bubble collapse, magnetohydrodynamics [13] and so on [14]. Furthermore, we have already succeeded in applying the CIP method to the Fokker Planck equation for plasma physics [15]. Nakamura and Yabe established the hyper-dimensional Vlasov-Poisson equation solver based on the CIP method, and Kondoh studied interaction between femtosecond-laser and matter both in microscopic and macroscopic levels using the CIP method [16].

During the development of the CIP method, the Soroban grid was proposed to achieve local mesh refinement (LMR) keeping higher-order accuracy by Yabe et. al [17]. The Soroban grid consists of lines and grid points in two dimensions, but the extension of Soroban grid to multidimensions such as six-dimensional Boltzmann equation is straightforward.

There are several merits to use the Soroban grid in the Boltzmann equation. (1) The range of velocity space can vary in time and space in accordance with the velocity space spread by the heating or acceleration. The particle code has great advantage in this respect since the particle can have its own velocity without velocity grid. Since the Soroban grid points in the velocity space can move independently from spatial grid points, the flexibility to trace such change in velocity space will be attained like in the particle code. (2) The local refinement is inevitable to treat the shock wave and other discontinuities. The Soroban grid can concentrate the grid to such discontinuities independently from the velocity space. (3) Even with such arbitrary grid points, higher order accuracy is well

preserved. (4) Since the computation of grid movement and subsequent extra computation are very effective, dynamical grid adjustment in time is economical. (5) Large CFL computation is possible and hence the time step limitation by large-velocity particle is removed. Usually the distribution at large velocity is negligibly small and it is a waste of time if the time step is determined from this part.

We have already applied the Soroban-grid CIP to a simple example, free-streaming in one-(space) dimensional Vlasov equation whose collision term is zero. It was shown that the recurrence phenomena intrinsic in the finite difference method can be avoided by the Soroban grid [19].

This paper presents the applications of the Soroban-grid CIP to rarefied gas dynamics. In Section 2, we briefly review the CIP method and the Soroban grid. Section 3 is devoted to the application of the Soroban-grid CIP to the Bhatnagar-Gross-Krook (BGK) equation [20]. The gas is assumed to be one dimension, i.e., the velocity distribution function depends on the x direction, three velocity components and time. Two typical calculations including shock tube problem and wall heating in two-dimensional phase space are examined and discussed. Section 4 is devoted to the conclusion and the future plans.

2 Numerical technique

2.1 The principle of the CIP method

Let us briefly describe the numerical technique of the CIP method. The one-dimensional advection equation is given by

$$\frac{\partial f}{\partial t}+u\frac{\partial f}{\partial x}=0, \tag{2.1}$$

and the Boltzmann equation is merely the six-dimensional extension of this equation.

Before proceeding further, let us explain the one-dimensional CIP scheme. When velocity u is constant and the initial condition of $f(x,t=0)$ is $F(x)$, the analytical solution of f in Eq. (2.1) can be readily described as $f(x,t)=F(x-ut)$, which means a simple translational motion of a wave. Even if u depends on x and t, this solution is approximately correct in a very short time Δt, that is, $f(x,t+\Delta t)\approx f(x-u\Delta t,t)$. All kinds of semi-Lagrangian methods such as linear, quadratic Lagrange, cubic Lagrange, and so on employ such Lagrangian invariant solution. Therefore, the CIP method is recognized to be a family of semi-Lagrangian scheme.

Unlike conventional semi-Lagrangian schemes, the CIP method uses the spatial derivative of f as well and such interpolation belongs to the Hermite spline interpolation. Let us differentiate Eq. (2.1) with spatial variable x, then we get

$$\frac{\partial g}{\partial t}+u\frac{\partial g}{\partial x}=-\frac{\partial u}{\partial x}g, \tag{2.2}$$

where g stands for the spatial derivative of $f(=\partial f/\partial x)$. In the simplest case that the velocity u is constant, Eq. (2.2) coincides with Eq. (2.1) and represents the propagation of spatial derivative with a velocity u. In this way, we can trace the time evolution of f and g on the basis of Eqs. (2.1) and (2.2).

If two values of f and g are given at two grid points, the profile between these points can be interpolated by cubic polynomial $F(x)=ax^3+bx^2+cx+d$. Thus, the profile at $n+1$ step can be obtained transporting the profile by $u\Delta t$ like $f^{n+1}=F(x-u\Delta t)$, $g^{n+1}=dF(x-u\Delta t)/dx$. Let

$$a_i=\frac{g_i+g_{iup}}{D^2}+\frac{2(f_i-f_{iup})}{D^3},\qquad b_i=\frac{3(f_{iup}-f_i)}{D^2}-\frac{2g_i+g_{iup}}{D}. \tag{2.3}$$

Then

$$\begin{aligned} f_i^{n+1}&=a_iX^3+b_iX^2+g_i^nX+f_i^n,\\ g_i^{n+1}&=3a_iX^2+2b_iX+g_i^n, \end{aligned} \tag{2.4}$$

where $X=-u\Delta t$ and the supersubscript "n" indicates the time step. Here, $iup(=i-sgn(u_i))$, $sgn(u_i)=1\,(u_i\geq 0)$, $-1\,(u_i<0)$, $D=-\Delta x\cdot sgn(u_i)$. Thus the function value and its spatial derivative at the next time step $n+1$ are explicitly given.

It is possible to extend the scheme to more than one dimension with a directional-splitting or non-directional-splitting technique. Let us first consider a two-dimensional hyperbolic equation in the Cartesian coordinates (x,y):

$$L(f)\equiv\frac{\partial f}{\partial t}+(\mathbf{u}\cdot\nabla)f=G, \tag{2.5}$$

where the velocity $\mathbf{u}=(u,v)$, $\nabla=(\partial/\partial x,\partial/\partial y)$. Eq. (2.5) is the same as the Boltzmann equation in two-dimensional phase space, that is, y and G are equivalent to velocity space coordinate and collision term, respectively. The following discussion can be applied to more than two dimensions in the same way.

First, we consider the case of $G=0$. The CIP method uses the first spatial derivatives $\partial f/\partial x$ and $\partial f/\partial y$ to make cubic-interpolation, and these equations are derived from Eq. (2.5) by $\partial_x L(f)=0$ and $\partial_y L(f)=0$. In other words, the first spatial derivatives must also be determined consistently with the master equation like one-dimensional case. However, it is not practical and economical to straightforwardly extend non-directional-splitting technique to six dimensions because of complexity of the six-dimensional cubic polynomial.

Nakamura and Yabe [15] proposed a simple scheme to extend the CIP to six dimensions by a directional splitting technique in the Cartesian grid. Such splitting technique was used in Boltzmann and BGK equations by Desvillettes et. al [23]. This scheme has a very good property in extending it to unstructured grid like the Soroban grid.

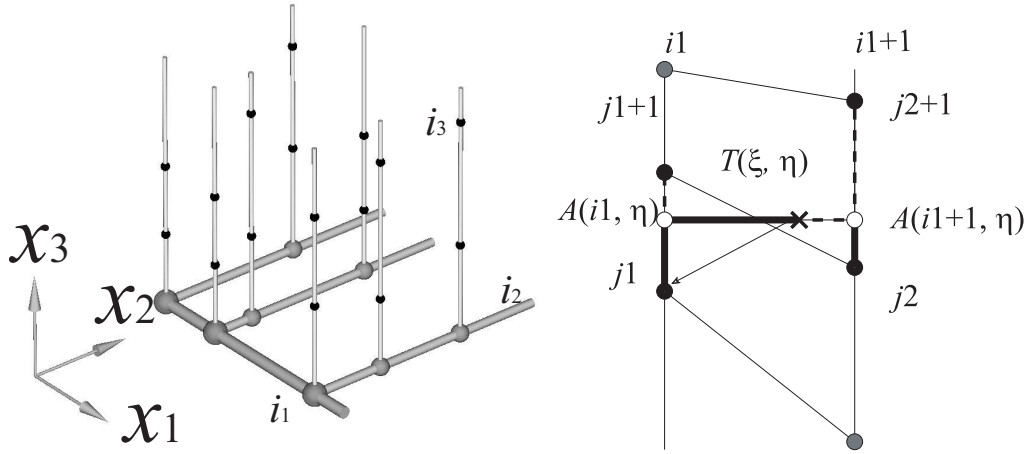

Figure 1: (Left) Soroban grid arrangement. (Right) Close view on a two-dimensional plane. Closed circles represent grid points.

2.2 The principle of Soroban grid

When the CIP scheme is applied to curvilinear system, the third-order accuracy that was achieved in uniform mesh is severely deteriorated and is degraded to the first-order in the deformed mesh [17]. Therefore the degradation of accuracy by introducing curvilinear coordinate would cancel the advantage of the CIP method that has originally the third order accuracy in time and space.

In order to resolve such difficulty, the CIP method has recently been upgraded to include the adaptive grid that guarantees the high-order accuracy as well as robustness. The new grid is named Soroban grid [17].

The schematic of the Soroban grid is shown in Fig. 1. The grid system consists of the straight lines and grid points moving along these lines like abacus- Soroban in Japanese. Planes also move in parallel in three-dimension. The length of each line and the number of grid points in each line can be different.

In order to understand how to solve the advection equations with the Soroban grid, let us consider a part of the Soroban grid shown in Fig. 1 (right) on a two dimensional plane for simplicity, where the vertical mesh (y-direction) is the straight line, while the grid points move along each line. Let (x_i,y_j) be the grid point which is to be updated. If the upstream departure point T is given as $(\xi,\eta)=(x_i-u\Delta t,y_j-v\Delta t)$, at first one pair of lines satisfying $x_{i1}<\xi<x_{i1+1}$ is searched. We should remind that x_i can be far from x_{i1} and x_{i1+1} so that large CFL$(u\Delta t/\Delta x,v\Delta t/\Delta y)$ computation is possible.

Next, two pairs of points satisfying $y_{j1}<\eta<y_{j1+1}$ and $y_{j2}<\eta<y_{j2+1}$ are searched along two lines at $x=x_{i1}$ and $x=x_{i1+1}$, respectively. The interpolation in this configuration can be performed as follows. At first, one-dimensional CIP is applied to the vertical straight line(y-direction) giving $A_{i1,\eta}$ and $A_{i1+1,\eta}$, and then T is given by one-dimensional CIP along the straight line connecting $A_{i1,\eta}$ and $A_{i1+1,\eta}$ in the x-direction. We have to pay

attention to spatial derivatives $\partial f/\partial x(\equiv g_x)$ and $\partial f/\partial y\left(\equiv g_y\right)$. As for y-direction, since f and g_y are transported along lines, A and only $\partial A/\partial y\left(=\partial_y A\right)$ are readily obtained by the CIP. In getting T by using cubic interpolation function along the straight line connecting $A_{i1,\eta}$ and $A_{i1+1,\eta}$ in the x-direction, we need some method to estimate $\partial A/\partial x(=\partial_x A)$ at the location of $A_{i1,\eta}$ and $A_{i1+1,\eta}$.

The previous paper [21] proposed to use the linear interpolation in getting $\partial A/\partial x$ from the gradients at two neighboring points along the line because the derivative in the direction perpendicular to the propagating direction is not sensitive and hence can be estimated roughly by the linear interpolation. Such a splitting scheme is called the "Type-M" scheme.

Although the Type-M scheme is sufficient for many applications, a little more accurate scheme is possible at the price of memory requirement. This scheme was proposed by Aoki [22] and we call it "Type-C" scheme. In this scheme, independent variables are f, $\partial_x f$, $\partial_y f$ and $\partial_{xy} f\left(=\partial_x\partial_y f=\partial_y\partial_x f\right)$ in two dimensions. For example, instead of using linear interpolation for $\partial_x f$ in y-direction, the one-dimensional CIP scheme is applied to the advection of $(\partial_x f)$ and $\partial_y(\partial_x f)$. The same can be said of x-direction, that is, the one-dimensional CIP scheme is applied to the advection of $\left(\partial_y f\right)$ and $\partial_x\left(\partial_y f\right)$.

It is very important to note that the number of grid points along each j line can be different. Corresponding 4 points $j1$, $j1+1$, $j2$, $j2+1$ including (ξ,η) point can be numerically searched. Most efficient method for finding the grid points in nonuniform mesh was proposed in [18]. By this method, the grid belonging to the upstream departure point is readily found with only one indexing procedure.

Since this scheme uses only the one-dimensional CIP method without coordinate transformation, it is able to keep the third order accuracy in time and space even in a deformed mesh [17]. The advantage of Type-M appears in the improved adaptive grid movement and local mesh-refinement.

As for the application of the Soroban grid to non-advection phase that include collision term in the BGK equations, we will not discuss it in this paper because it has been described in previous papers [9, 17].

2.3 Soroban grid and accuracy

For the benchmark test, we adopted a mesh system shown in Fig. 2 (the same test as [17]). This mesh is symmetrical at the center in the x-direction. The leftmost region is rectangular and its size is 40×96 and $\Delta x=\Delta y=\Delta x_0$. The length of the second trapezoidal region is 56 in x-direction and the mesh size Δx in x-direction is the same as that in the first region. The mesh size in y-direction changes linearly reaching $\Delta y=RATE\times\Delta x_0$ at the center. The benchmark test was done for three cases $RATE=0.5$, 1.0, 1.5 by changing the mesh size as $\Delta x_0=8$, 4, 2, 1 for measuring accuracy. $RATE=1.0$ corresponds to the uniform region and $RATE=0.5$ gives a shape like Fig. 2.

Let us summarize the mesh arrangement denoting the mesh size as $\Delta x_0=8/k$ ($k=1$, 2, 4, 8 is used to change the mesh size) and setting the grid point be (i,j), where $i=$

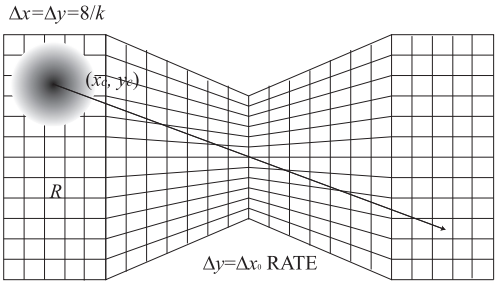

Figure 2: Grid arrangement and initial profile for benchmark test.

$0,1,\cdots,24k$, $j=0,1,\cdots,12k$. Then

$$\begin{aligned}
&\Delta y=\Delta x_0, \quad i=0,\cdots,5k,\\
&\Delta y=\Delta x_0\times(1+(RATE-1)\times(i-5k)/7k), \quad i=5k,\cdots,12k,\\
&\Delta y=\Delta x_0\times(1+(RATE-1)\times(19k-i)/7k)), \quad i=12k,\cdots,19k,\\
&\Delta y=\Delta x_0, \quad i=19k,\cdots,24k,
\end{aligned} \tag{2.6}$$

where $\Delta x=\Delta x_0$ is a fixed constant and Δy is a constant along each vertical line, $(i,j)=(0,0)$ is the origin and $(i,j)=(96,48)$ is the center.

We calculate the propagation of a profile

$$f(x,y)=\begin{cases}\dfrac{1+\cos\left(\pi\sqrt{(x-x_c)^2+(y-y_c)^2}/R\right)}{2}, & (x-x_c)^2+(y-y_c)^2<R^2,\\ 0, & \text{otherwise},\end{cases} \tag{2.7}$$

and $R=15$, $(x_c,y_c)=(16,80)$, $u=0.1$, $v=-0.04$, $\Delta t/\Delta x_0=2$ are used for the test run. The initial values for the derivatives are estimated by analytically differentiating Eq. (2.7). At $t=1600$, the initial profile moves to the opposite side of Fig. 2 and the numerical error is estimated by Eq. (2.8)

$$\epsilon\equiv\frac{\sqrt{\sum\left(f_{Num}-f_{exact}\right)^2}}{\sum f_{exact}}, \tag{2.8}$$

where f_{Num} is the numerical result and f_{exact} is the exact solution, and ϵ in each scheme is shown in Fig. 3. Both Type-M and Type-C have approximately the 3rd-order accuracy. The 3rd-order accuracy of the Type-C is as is expected because it uses the CIP procedure all through the process. Although the Type-M uses the first-order scheme (linear interpolation) in estimating the derivative in perpendicular direction, it gives the accuracy better than 2nd-order.

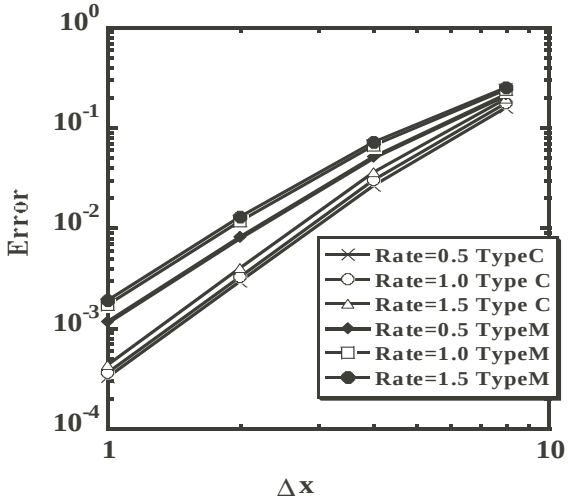

Figure 3: The numerical error ϵ for different grid shape with Type-M and Type-C.

2.4 Moving adaptive Soroban grid

Here, we shall discuss the possibility to use the Soroban grid as for the adaptive grid to the moving body. We remind that all the discussion can be straightforwardly applied to multi-dimensions. At first, let us consider one-dimensional case. For the simplest choice of the monitoring function to the variation, we can use the following quantity:

$$M(x,t) \equiv \sqrt{1+\alpha\left(\frac{\partial f}{\partial x}\right)^2+\beta\left(\frac{\partial^2 f}{\partial x^2}\right)^2}, \tag{2.9}$$

where the two parameters α and β can be chosen depending on problems of concern. The monitoring function M given by Eq. (2.9) becomes large for larger gradient region. Since the Soroban grid is straight in one-direction, it is much easier to generate the adaptive grid points along the line.

The reorganization of the grid point is easily performed by accumulated monitoring function $I(x)$ as shown in Fig. 4. If we divide the accumulated function into equal pieces, the x-coordinate of boundary for each piece gives the grid points. It is easy to observe that the size of grid Δx becomes small where monitoring function M is large. Therefore, grid points are concentrated on the region where spatial gradient is large (like boundary layer), and this procedure is repeated in every time step.

In the two-dimensional mesh shown in Fig. 5, mesh moving is performed as follows.

1. Calculate $M(y,t)$ along each line
2. Generate the points along each line.
3. Calculate the average $M(x,t)$ from all the points along each line.
4. Move the lines.

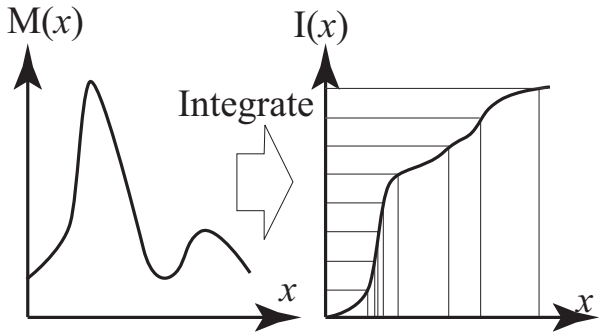

Figure 4: Accumulated monitoring function $I(x)$ is divided into equal pieces. The x boundary of each piece gives the grid point.

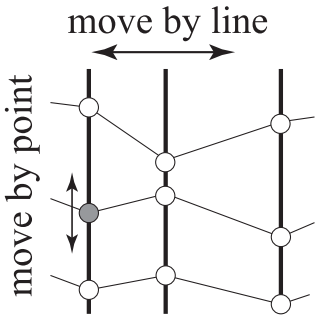

Figure 5: The straight lines can move in horizontal direction and grid points move along the straight lines.

The monitoring functions have been used in several preceding studies for generation of adaptive mesh [24–27], not only in Finite-Difference method but also Finite-Element or Finite-Volume Method [28, 29]. In addition, there are some robust unstructured adaptive grid schemes applied to the BGK equation [31].

In the sense that we adopt the monitoring function, the Soroban-grid CIP method has a similarity in mesh generation to the other conventional adaptive mesh methods. However, distinct difference between the Soroban grid and the preceding methods is that the Soroban grid does not use the coordinate mapping between the physical domain Ω_p and the computational domain Ω_c so that the third-order accuracy can be obtained even with unstructured Soroban-grid as mentioned in Section 2.3. The Soroban grid is a kind of unstructured grid but simultaneously it has a regular structure like the Cartesian grid. Therefore, only one-dimensional monitoring function like Eq. (2.9) is sufficient for any multi-dimensional calculations with directional splitting. In addition, the combination of the Soroban grid and the semi-Lagrangian approach becomes very efficient because finding the upstream points for large CFL is easily performed in such semi-regular grid arrangement. It is also important to note that the grid movement and advection procedure can be performed by only one procedure [32, 33]. Suppose that we set a new grid point, the updated value at this point after advection can be found by searching an up-

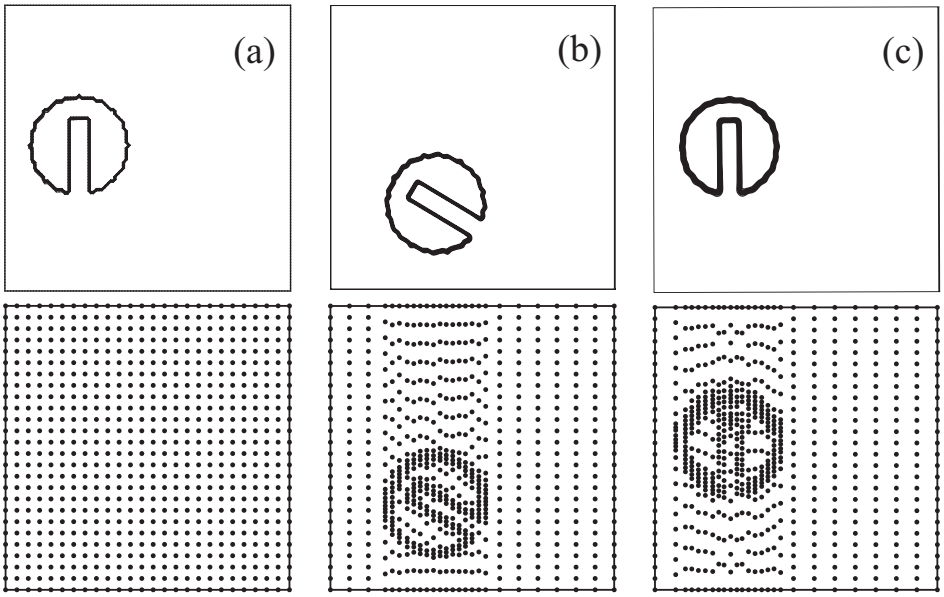

Figure 6: Solid body revolution. Density contour and grid points. (a) $t=0$, (b) $t=133$, (c) $t=800$.

stream point of this new grid, interpolating the value from neighbouring old grid points, and transporting the value to the new grid point. Thus grid movement and advection procedure are performed by one procedure. However, some sophistications proposed in previous papers [25,26,30] would improve the generation of the Soroban grid.

This moving grid scheme is applied to the solid body revolution proposed by Zalesak [34]. The mesh of 101×101 is used and the rotation center is located at $(x_c,y_c)=(50,50)$. The initial profile is

$$f(x,y)=\begin{cases} 1, & R\leq 17 \text{ and } (|x-26|>3 \text{ or } y>60), \\ 0, & \text{otherwise}, \end{cases} \tag{2.10}$$

where $R=\sqrt{(x-26)^2+(y-51)^2}$. The mesh size is initially $\Delta x=\Delta y=1.0$. The time step is fixed to $\Delta t=1$, and the parameters α and β in (2.9) are chosen as $\alpha=1$ and $\beta=0.3$. Revolution speed is set so that the revolution is completed after 800 steps, namely,

$$u=-2\pi(y-y_c)/800, \quad v=2\pi(x-x_c)/800. \tag{2.11}$$

Fig. 6 shows the contour where increment is 0.1 and the corresponding grid points are depicted. It is important to note that the time step is fixed to $\Delta t=1$, thus as the mesh is moving as shown in the figure, the mesh can be very small and the CFL value can easily exceed 1. In this simulation, we do not need the information of the connectivity between two points in different lines. The upstream departure point is searched along the line and

can be separated by several mesh size from the terminal point. Actually, the maximum CFL was 22 at the locally refined mesh.

The extension of the Soroban grid to more than two dimensions was described in [32, 33]. Note that selection of a quantity f for monitoring function Eq. (2.9) can be different in each $M(x,t)$ or $M(y,t)$.

The possibility to use the Soroban grid as the adaptive grid to the moving body has already been discussed in [17]. It is based upon the monitoring function to the variation, and local mesh refinement can be achieved. The drawback was that the Soroban grid thus generated would not be smooth because the grid size would be automatically determined by the monitoring function and thus the ratio of grid size would become extremely large.

One way to avoid such drawback is to set the maximum value of monitoring function. For example, we do not use Eq. (2.9) $M(x,t)$, but

$$M(x,t)_{used} = \min\{r \equiv \Delta x_{max}/\Delta x_{min}, M(x,t)\} \tag{2.12}$$

is used, where $r \equiv \Delta x_{max}/\Delta x_{min}$ means the ratio between the maximum and minimum grid sizes. After predicting the magnitude of spatial derivatives, we can choose the two parameters α and β in Eq. (2.9) so that the monitor function stays in the range of r. Another way is to smooth the spatial derivatives in the monitoring function [32, 33]. This method may be more effective for the Soroban grid and is now under development.

The CIP method is suitable for this mesh system because it uses only two stencils to make up cubic-interpolation function, and the calculation of large CFL(>10) at locally refined mesh is easily performed. Mesh generation and searching of upstream departure point are very simple and almost mesh-free treatment is possible.

3 Soroban-grid CIP for BGK equation

3.1 Formulation of the problem : Notations and basic equations

The standard Boltzmann equation for velocity distribution function $f(\mathbf{x},\mathbf{v},t)$ in phase space $\mathbf{x}=(x_1,x_2,x_3)$ and velocity $\mathbf{v}=(v_1,v_2,v_3)$ is written as

$$\frac{\partial f}{\partial t} + (\mathbf{v}\cdot\nabla_{\mathbf{x}})f + \left(\frac{\mathbf{F}}{m}\cdot\nabla_{\mathbf{v}}\right)f = \left(\frac{\partial f}{\partial t}\right)_{coll}, \tag{3.1}$$

where $\nabla_{\mathbf{x}} \equiv (\partial/\partial x_1, \partial/\partial x_2, \partial/\partial x_3)$, $\nabla_{\mathbf{v}} \equiv (\partial/\partial v_1, \partial/\partial v_2, \partial/\partial v_3)$, $\mathbf{F}$ is the force and m is the mass of particle, and $(\partial f/\partial t)_{coll}$ is the collision term. Since the CIP can accurately describe the advection process even with coarse grid, it is possible to solve six-dimensional phase space in the Eulerian grid system. In plasma simulation, Landau damping was correctly described even with ten grids in the whole velocity space by the CIP method and six-dimensional computation has been performed only with one personal computer [15].

As for applications of the standard Boltzmann equation to rarefied gas, the Bhatnagar-Gross-Krook (BGK for short) has been frequently used in a number of recent literatures.

Attempts to derive it or justify the model have been made in a number of previous papers and the BGK equation is recognized to be an essential model of the standard Boltzmann equation. In this paper, we focus on the one-(space) dimensional BGK equation because it is sufficient to show the effectiveness and possibility of the Soroban-grid CIP method and general establishments to the standard Boltzmann equations will appear in future papers.

The BGK equation in one dimension $(\partial/\partial x_2=\partial/\partial x_3=0)$ with free force $(\mathbf{F}=0)$ is

$$\frac{\partial f}{\partial t}+v_1\frac{\partial f}{\partial x_1}=A_c\rho(f_e-f)\ (=\nu(f_e-f)), \tag{3.2}$$

where A_c is a constant parameter, ρ is the density, and the collision frequency is given by $\nu=A_c\rho$. f_e is the local Maxwellian distribution and the collision term on the right-hand side of Eq. (3.1) is replaced by a term proportional to the difference between the current distribution function and the local Maxwellian distribution function.

$$f_e=\frac{\rho}{(2\pi RT)^{3/2}}\exp\left(-\frac{c^2}{2RT}\right). \tag{3.3}$$

Here, ρ and T, respectively, denote the density and temperature of gas flow, R is the specific gas constant. c represents the magnitude of the thermal velocity, that is, $c^2=c_1^2+c_2^2+c_3^2$, where $c_i=v_i-u_i$ $(i=1,2,3)$ and u_i is the mean velocity along i-direction.

The BGK equation (3.2) is an idealized model of the full Boltzmann equation and it is well-known that the following hydrodynamics equations for continuum flow can be easily derived by taking the moment of distribution function:

$$\frac{\partial \mathbf{a}}{\partial t}+\mathbf{u}\cdot\nabla\mathbf{a}=\mathbf{S}, \tag{3.4}$$

where $\mathbf{a}=(\rho,\mathbf{u},p)$, $\mathbf{S}=(-\rho\nabla\cdot\mathbf{u},-\nabla p/\rho,-\gamma p\nabla\cdot\mathbf{u})$, p is the pressure and γ is the specific heat ratio.

However, in the Chapman-Enskog expansion, the BGK model corresponds to the Prandtl number $Pr=\mu C_p/K$ of unity, where μ is the viscosity coefficient and K is the heat conduction. The modified BGK equation (BGK-ES(ellipsoidal statistical) model equation, for short) has been proposed [35], and the local Maxwellian Eq. (3.3) has to be replaced by Eq. (3) in [37] in order to deal with any Prandtl numbers. Although this paper does not employ the BGK-ES model, the application of the Soroban-grid CIP to this model is straightforward as well.

In one space dimension (x_1), the distribution function f is in general a function of five variables: x_1, t, and three velocity components v_1, v_2, v_3. In this case, however, a simplification is possible [2] so that the procedure can be reduced to the solution of the following two functions of the x_1 and v_1 components:

$$g(x_1,v_1,t)\equiv\int_{-\infty}^{-\infty}\int_{-\infty}^{-\infty}f dv_2dv_3,\quad h(x_1,v_1,t)\equiv\int_{-\infty}^{-\infty}\int_{-\infty}^{-\infty}\left(v_2^2+v_3^2\right)f dv_2dv_3. \tag{3.5}$$

Integrating with respect to v_2 and v_3 and using Eq. (3.5), Eq. (3.2) can be reduced to the following equivalent system:

$$\frac{\partial}{\partial t}\begin{pmatrix} g \\ h \end{pmatrix} + v_1 \frac{\partial}{\partial x_1}\begin{pmatrix} g \\ h \end{pmatrix} = A_c \rho \begin{pmatrix} g_e - g \\ h_e - h \end{pmatrix}, \tag{3.6}$$

where the density ρ, the mean velocity u_1 in the x_1-direction and the temperature T are obtained as

$$\rho = \int_{-\infty}^{\infty} g dv_1, \quad u_1 = \frac{1}{\rho}\int_{-\infty}^{\infty} v_1 g dv_1, \quad 3RT = \frac{1}{\rho}\int_{-\infty}^{\infty} \Big((v_1 - u_1)^2 g + h \Big) dv_1, \tag{3.7}$$

and the pressure $p = \rho RT$.

Eq. (3.6) is put into nondimensional form by introducing the normalizing quantities such as the reference density ρ_0 and the temperature T_0, the initial mean thermal velocity $\sqrt{2RT_0}$ as the reference velocity, the reference length l_0 which is set to the mean free path of the gas molecules in equilibrium state at rest with T_0. The distribution functions g and h are also normalized by $\sqrt{2\pi RT_0}$. Therefore, nondimensionalized BGK equation can be represented as

$$Sh\frac{\partial}{\partial t}\begin{pmatrix} g \\ h \end{pmatrix} + v_1 \frac{\partial}{\partial x_1}\begin{pmatrix} g \\ h \end{pmatrix} = k\rho \begin{pmatrix} g_e - g \\ h_e - h \end{pmatrix}, \tag{3.8}$$

where

$$\rho = \frac{1}{\sqrt{\pi}}\int_{-\infty}^{\infty} g dv_1, \quad u_1 = \frac{1}{\rho\sqrt{\pi}}\int_{-\infty}^{\infty} v_1 g dv_1, \quad T = \frac{2}{3\sqrt{\pi}\rho}\int_{-\infty}^{\infty} \Big((v_1 - u_1)^2 g + h \Big) dv_1, \tag{3.9}$$

and pressure $p = \rho T/2$. g_e and h_e that correspond to the local Maxwellian distribution are

$$g_e(x_1, v_1, t) = \frac{\rho}{\sqrt{T}} \exp\left(-\frac{(v_1 - u_1)^2}{T} \right), \quad h_e(x_1, v_1, t) = \rho\sqrt{T} \exp\left(-\frac{(v_1 - u_1)^2}{T} \right). \tag{3.10}$$

Note that we employ the same notation both for the un-normalized and normalized values but it should not cause confusion. $Sh = l_0/\left(t_0\sqrt{2RT_0}\right)$ is called the Strauhal number, in which t_0 is the reference time. $k \equiv A_c \rho l_0/\sqrt{2RT_0}$ is the inverse of Knudsen number and is given by the ratio between mean free path and reference length. Here, $Sh = 1.0$ and k is chosen depending on problems of concern in this paper.

The initial value problems of two simultaneous BGK equations (3.8) to (3.10) are solved by the CIP method.

Solving BGK equation, some difficulty appears from the collision term because the analytical form of the local Maxwellian f_e is not necessarily the correct approximation to the conservative properties Eq. (3.7) owing to the numerical discretization error. In this paper, the discrete-velocity model (DVM) [36], which solves a discrete approximation of the local equilibrium Eq. (3.3) defined by a minimum entropy principle, is employed for the collision operator. Although the DVM was used for the original BGK equation (3.2), it can be easily applied to (g_e, h_e) in two simultaneous BGK equations (3.8).

3.2 One-dimensional SOD shock-tube problem

We here apply the Soroban-grid CIP method to the one-dimensional examples of the BGK equation tha have been used as benchmark tests by preceding papers. The first example is a SOD shock tube problem [2]. It is well known as the Riemann problem and the initial discontinuity generates some discontinuities like shock front, contact discontinuity and rarefaction wave. Especially, the structure of normal shock waves has been studied as one of the most fundamental nonlinear problems in rarefied gas dynamics with theories, experiments and numerical simulations [2,7,37].

Consider a system with a uniform-temperature region initially with a high-density layer ρ_L placed on the left and a low-density layer ρ_R on the right. The density (or pressure) ratio is 10:1, that is, $\rho_L/\rho_R=10.0\left(\equiv\alpha_\rho\right)$. Therefore, there is a discontinuity in distribution function g and h initially at $x_1=x_c(=L/2)$, where the system size L is $60l_0$ in the x_1-direction. The number of lines in the x_1-direction is 150 and $\Delta x_{ini}\equiv L/150=0.4$. The 60 grid points move along each line in velocity space v_1 from $-12(-v_{max})$ to $+12(+v_{max})$. The time interval Δt is fixed to $0.01\Delta x_{ini}$. The calculation is performed up to $t(/t_0)=15.0$.

The initial condition in normalized form is set to the Maxwellian in each region, having uniform temperature, and they are described as

$$g(x_1,v_1,t=0)=h(x_1,v_1,t=0)=\begin{cases}\exp\left(-v_1^2\right) & (x_1\geq x_c),\\ \alpha_\rho\exp\left(-v_1^2\right) & (x_1\leq x_c),\end{cases} \tag{3.11}$$

$$\frac{\partial g}{\partial v_1}(x_1,v_1,t=0)=\frac{\partial h}{\partial v_1}(x_1,v_1,t=0)=\begin{cases}-2v_1\exp\left(-v_1^2\right) & (x_1\geq x_c),\\ -2\alpha_\rho v_1\exp\left(-v_1^2\right) & (x_1\leq x_c),\end{cases} \tag{3.12}$$

$$\frac{\partial g}{\partial x_1}(x_1,v_1,t=0)=\frac{\partial h}{\partial x_1}(x_1,v_1,t=0)=0. \tag{3.13}$$

The function value and its derivatives at the boundaries $x_1=0$ and $x_1=\infty(=L)$ are fixed to the initial condition Eqs. (3.11) to (3.13).

In the applications of the Soroban grid, efficient moving of the Soroban grid is the key issue. In the present example, we had better choose different strategy in the x and v directions by selecting monitoring function $M_x(x_1,t)$ and $M_v(x_1,v_1,t)$ independently. $M_v(x_1,v_1,t)$ should be made with the velocity distribution function $g(x_1,v_1,t)$ because the number of grid points near the velocity boundary $v_1=\pm v_{max}$ can be reduced because of very small value of distribution function. In the x direction, however, it is better to make $M_x(x_1,t)$ with density $\rho(x_1,t)$ since some discontinuities in variables such as density $\rho(x_1,t)=\int_{-\infty}^{\infty}gdv_1$ will appear in space after integration of distribution function along v_1, so that we can trace not only shock front but also contact discontinuity.

Therefore, the following monitoring function $M_x(x_1,t)$ and $M_v(x_1,v_1,t)$ are proposed:

$$\begin{aligned}M_x(x_1,t)&=1+a_x\left|\frac{\partial\rho(x_1,t)}{\partial x_1}\right|+b_x\left|\frac{\partial^2\rho(x_1,t)}{\partial x_1^2}\right|,\\ M_v(x_1,v_1,t)&=1+a_v\left|\frac{\partial g(x_1,v_1,t)}{\partial v_1}\right|+b_v\left|\frac{\partial^2 g(x_1,v_1,t)}{\partial v_1^2}\right|,\end{aligned} \tag{3.14}$$

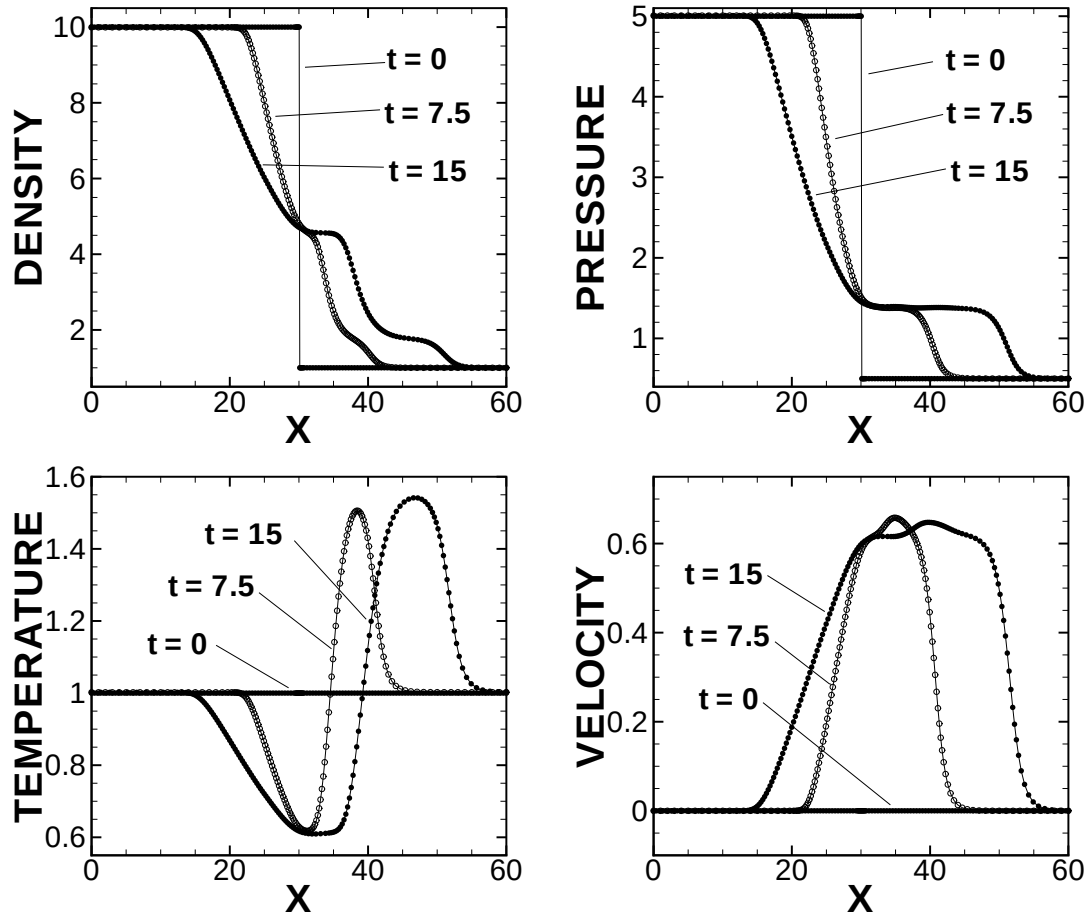

Figure 7: The time variation of density, temperature, velocity and pressure with Soroban-grid CIP in the case of $k=2/\sqrt{\pi}$.

where coefficients $(a_x,b_x)=(30.0,60.0)$ and $(a_v,b_v)=(0.1,0.0)$ are used. The maximum ratio of the grid size r in Eq. (2.12) is set to be 5.0 in both x_1 and v_1 directions.

Figs. 7 and 8 show the time evolution of the density ρ, mean velocity u_1, pressure p and temperature T profiles at various instants of time for two cases of $k=2/\sqrt{\pi}$ (rarefied flow) and $k=200/\sqrt{\pi}$ (continuum flow) in Eq. (3.8), respectively. Fig. 9 shows comparison of all macroscopic variables among analytical solution, Soroban-grid CIP and uniform-grid CIP in the case of $k=200/\sqrt{\pi}$. The solid line denotes the analytical solution of the shock-tube problem obtained using the Euler equations of gas dynamics of continuum flow [8, 38]. As clearly observed in Figs. 7 and 8, shock front, contact discontinuity and rarefaction wave become steep and approach to the analytical solution as the Knudsen number decreases from $1/k=\sqrt{\pi}/2$ to $1/k=\sqrt{\pi}/200$ as observed in [37], and therefore the Soroban-grid CIP method is proven to be valid for both continuum and

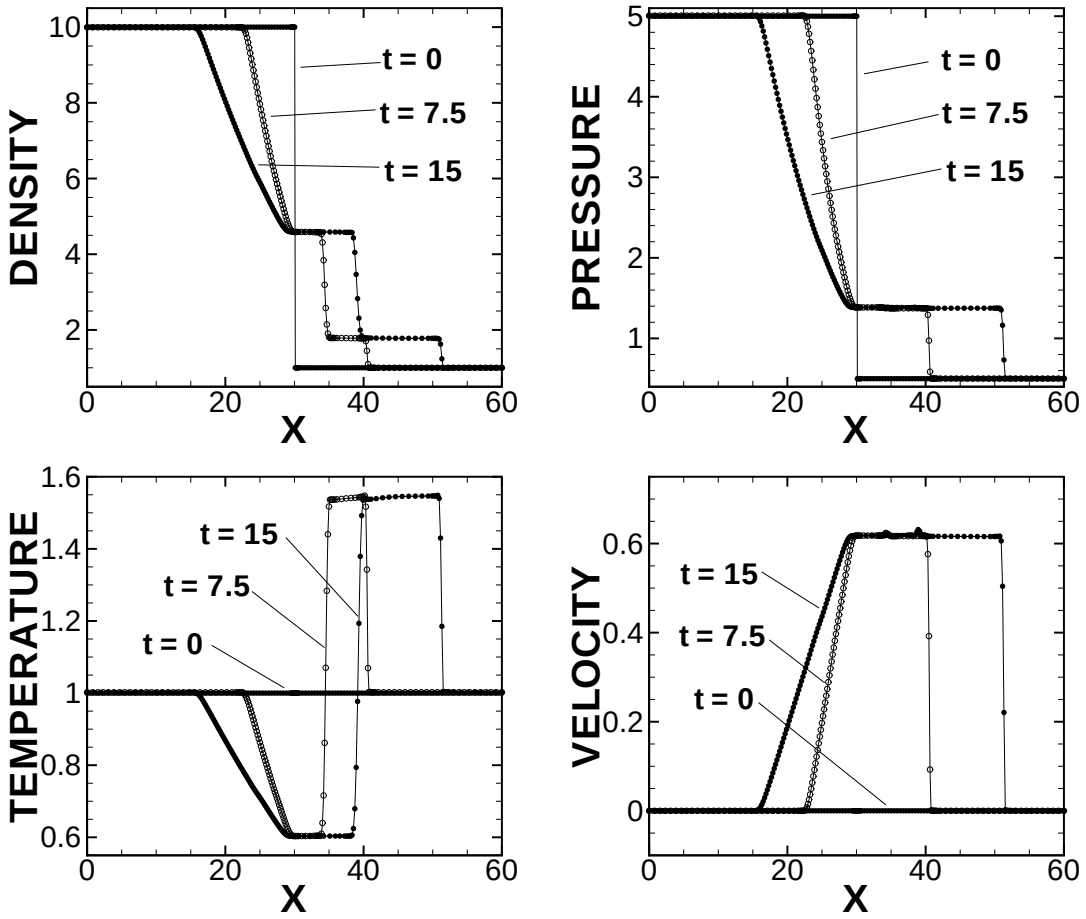

Figure 8: The time variation of density, temperature, velocity and pressure with Soroban-grid CIP in the case of $k=200/\sqrt{\pi}$.

rarefied flows.

Fig. 10 shows the time evolution of the distribution function g and the Soroban grid points in the case of $k=200/\sqrt{\pi}$. At $t=0$, $\partial g/\partial v_1$ in $(x_1 \geq x_c)$ is much smaller than that in $(x_1 \leq x_c)$, and therefore the concentration of the Soroban grid towards the center along the velocity space becomes prominent in $x_1 \leq x_c$. As the time proceeds, the concentrated Soroban grid moves following the movement of distribution function g, but still keeping a few grid points near the velocity space boundary $v_1 \sim \pm v_{max}$.

Fig. 11 depicts the comparison of the distribution function $g(x_1,v_1)$ between uniform grid and Soroban grid at $t=15$ in the case of $k=200/\sqrt{\pi}$. The Soroban-grid CIP describes the distribution function $g(x_1,v_1)$ more clearly than by uniform grid around $v_1=0$ axis.

Since monitoring function $M_x(x_1,t)$ is made with ρ, the resolution near shock front and contact discontinuity is better than that in the other part. Especially, in the case of

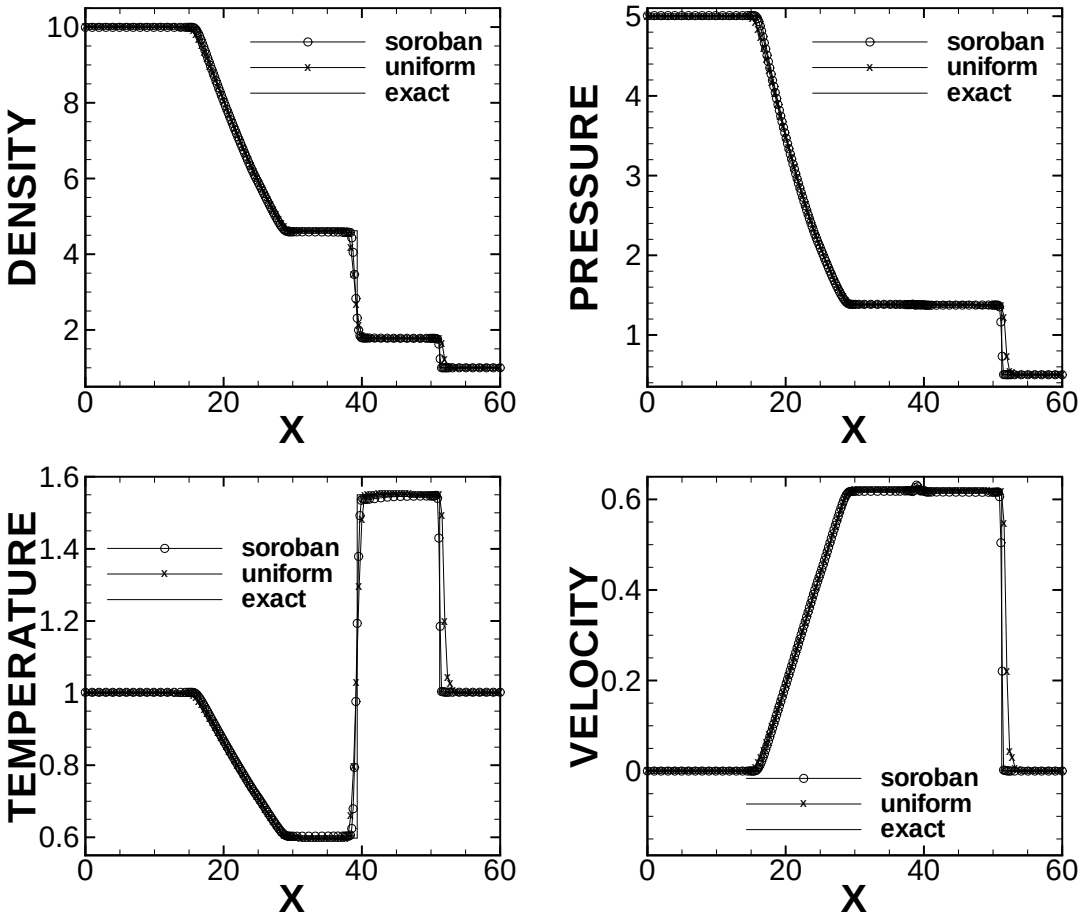

Figure 9: The comparison among analytical solution, Soroban-grid CIP and uniform-grid CIP in the case of $k=200/\sqrt{\pi}$.

continuum flow with small Knudsen number shown in Fig. 9, the numerical solution by the Soroban grid is improved significantly than that by the uniform grid. When the number of grid points in uniform grid increases, such difference should be reduced.

Actually, the result with the finer uniform grid with the number of lines 750 for $x=[0,60]$ in the x_1-direction and the number of grid points 150 for $v=[-6,6]$ in each line (v_1-direction) becomes very closer to the Soroban grid as shown in Fig. 12.

3.3 One-dimensional heating by wall

Next application is rarefied gas heated by a wall with higher temperature [39]. The region $(0<x_1\leq L)$ is filled with static $(u_1=0)$ rarefied gas $(k=2/\sqrt{\pi})$ with reference density ρ_0 and temperature T_0 at $t=0$, respectively. Therefore, the initial condition is simply

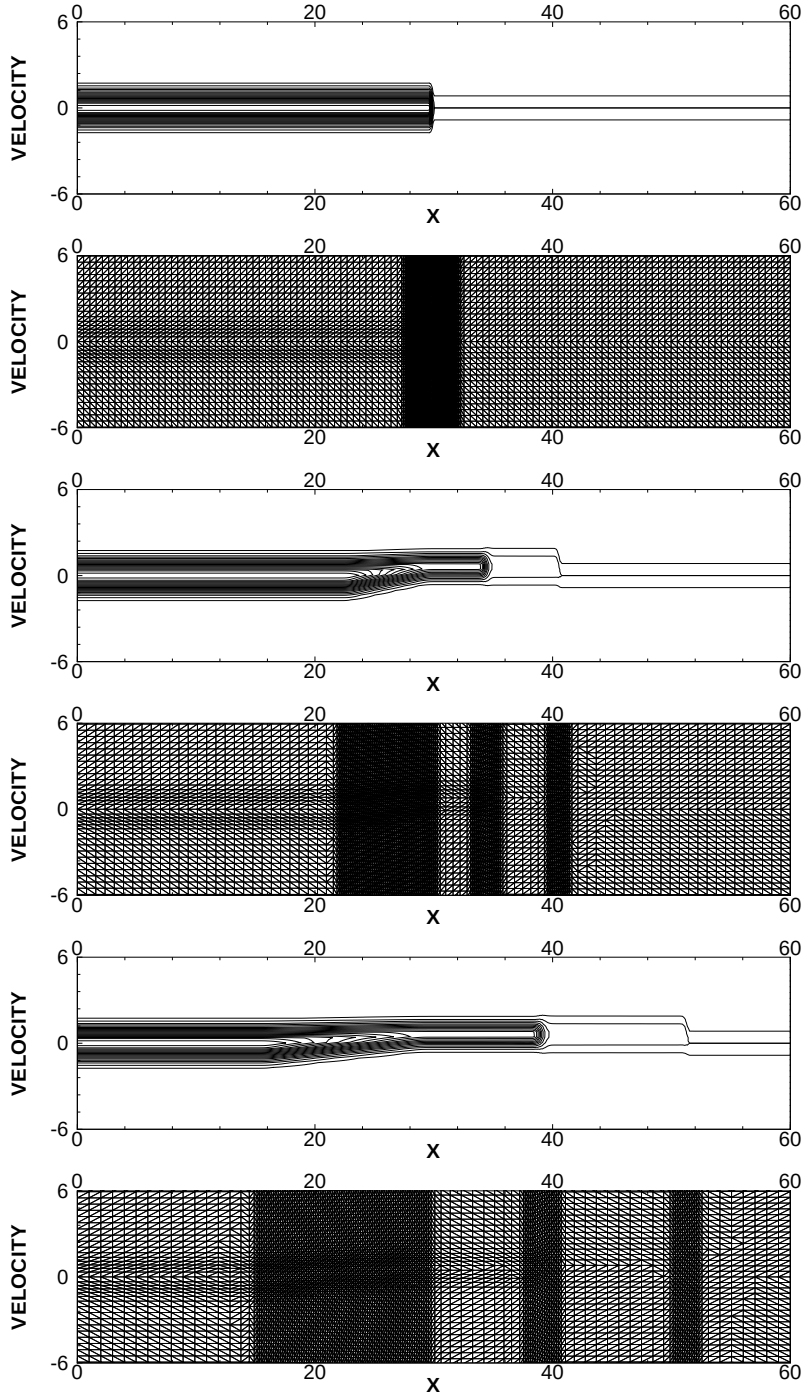

Figure 10: The distribution function $g(x_1,v_1)$ and Soroban grid at $t=0,7.5,15$ in the case of $k=200/\sqrt{\pi}$. Only the velocity range $v=[-6,6]$ is plotted while the calculation was performed in the range $v=[-12,12]$.

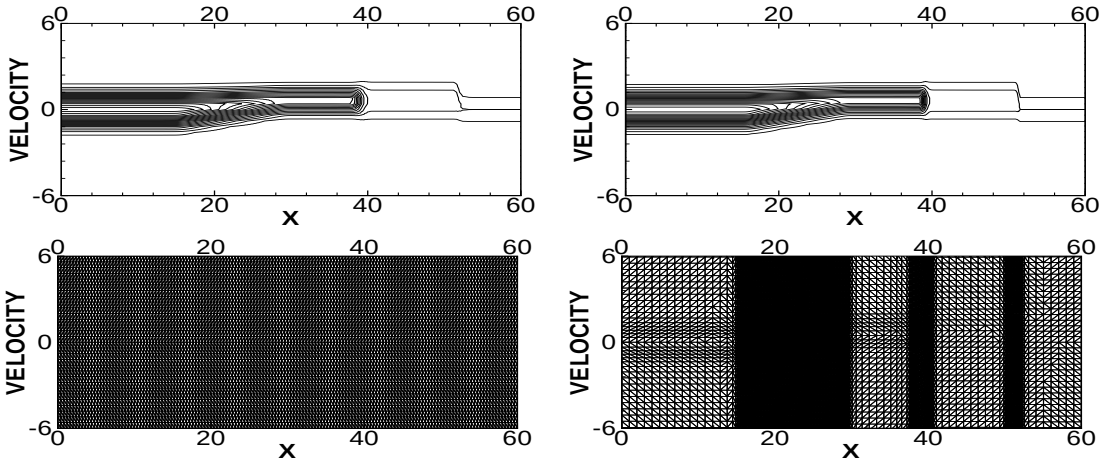

Figure 11: The comparison of the distribution function $g(x_1,v_1)$ between uniform grid (left column) and Soroban grid (right column) at $t=15$ in the case of $k=200/\sqrt{\pi}$. Only the velocity range $v=[-6,6]$ is plotted while the calculation was performed in the range $v=[-12,12]$.

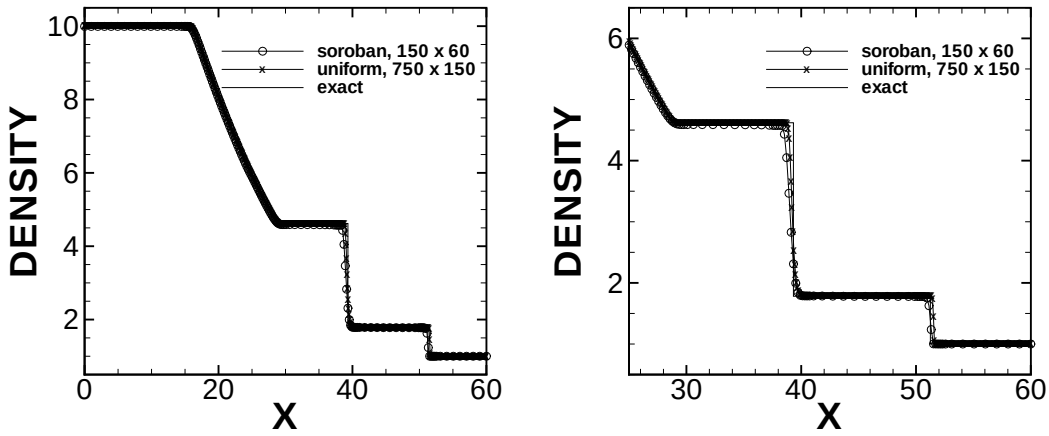

Figure 12: The comparison of density among the analytical solution, the Soroban-grid CIP$(150,60)$ for velocity range $v=[-12,12]$ and the finer uniform-grid CIP$(750,150)$ for velocity range $v=[-6,6]$ in the case of $k=200/\sqrt{\pi}$ at $t=15$: (left) whole view and (right) enlarged local view near two discontinuities.

described by the Maxwell distribution:

$$g(x_1,v_1,t=0)=h(x_1,v_1,t=0)=\exp\left(-v_1^2\right), \tag{3.15}$$

$$\frac{\partial g}{\partial v_1}(x_1,v_1,t=0)=\frac{\partial h}{\partial v_1}(x_1,v_1,t=0)=-2v_1\exp\left(-v_1^2\right), \quad (x_1\geq 0). \tag{3.16}$$

The boundary condition at $x_1=0$ is assumed to be the wall that is the diffuse reflection boundary with the temperature $T_1(=\alpha_T T_0)$ like heat source

$$g(0,v_1,t)=\frac{\rho_w}{\sqrt{\alpha_T}}\exp\left(-v_1^2\right), \quad h(0,v_1,t)=\rho_w\sqrt{\alpha_T}\exp\left(-v_1^2\right), \quad (v_1>0), \tag{3.17}$$

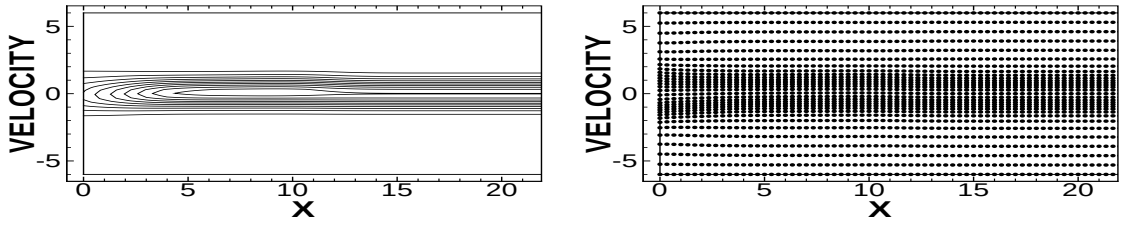

Figure 13: The distribution function $g(x_1,v_1)$ and Soroban grid near the wall $t=10.0$.

where ρ_w is the density that is determined by the distribution function of incident fluid to the wall,

$$\rho_w = -\sqrt{\frac{2}{\alpha_T}}\int_{-\infty}^{0} v_1 g(0,v_1,t)\,dv_1, \tag{3.18}$$

where $\alpha_T = 2.0$.

The system size is $100l_0$ and the velocity space is ranging from $-6(-v_{max})$ to $+6(+v_{max})$. The number of lines in the x_1-direction is 300 and the 30 grid points move along each line. The time interval Δt is fixed to 0.001. The parameters used for monitoring function in Eq. (3.14) are $(a_x,b_x)=(0.0,0.0)$ and $(a_v,b_v)=(3.0,0.4)$. The calculation is performed up to $t=80.0$.

Fig. 13 shows the distribution function $g(x_1,v_1,t)$ near the wall in phase space at $t=10.0$. The Soroban grid points are concentrated following the change of the distribution function.

Fig. 14 shows the time variations of the density, temperature, velocity and pressure. Heating on the wall increases pressure near the wall and the generated weak shock propagates as time goes on. However, since no flow comes from the wall, the density near the wall begins to decrease. Decreased density and no energy flow decrease peak pressure of the shock front as well, and rarefaction wave begins to follow the proceeding shock front.

4 Conclusion

Sone et. al [40] carried out accurate numerical analysis of evaporation and condensation on a plane condensed phase on the basis of the linearized Boltzmann equation for hard-sphere molecules with the finite difference method. They devised an efficient way to calculate the linearized collision integral by the matrix product of a universal collision kernel. This procedure can be directly employed in our scheme as well, and can be extended to describe the asymptotic behavior of a rarefied gas for small Knudsen numbers in evaporation and condensation problem.

The ultimate purpose is to establish the universal solver for the six-dimensional standard Bolztmann equation using the CIP method with the Soroban grid. Since the Soroban grid is capable of treatment like mesh-free schemes, it will be possible to set accurate boundary condition by the Soroban grid for arbitrarily shaped complex boundaries. Even

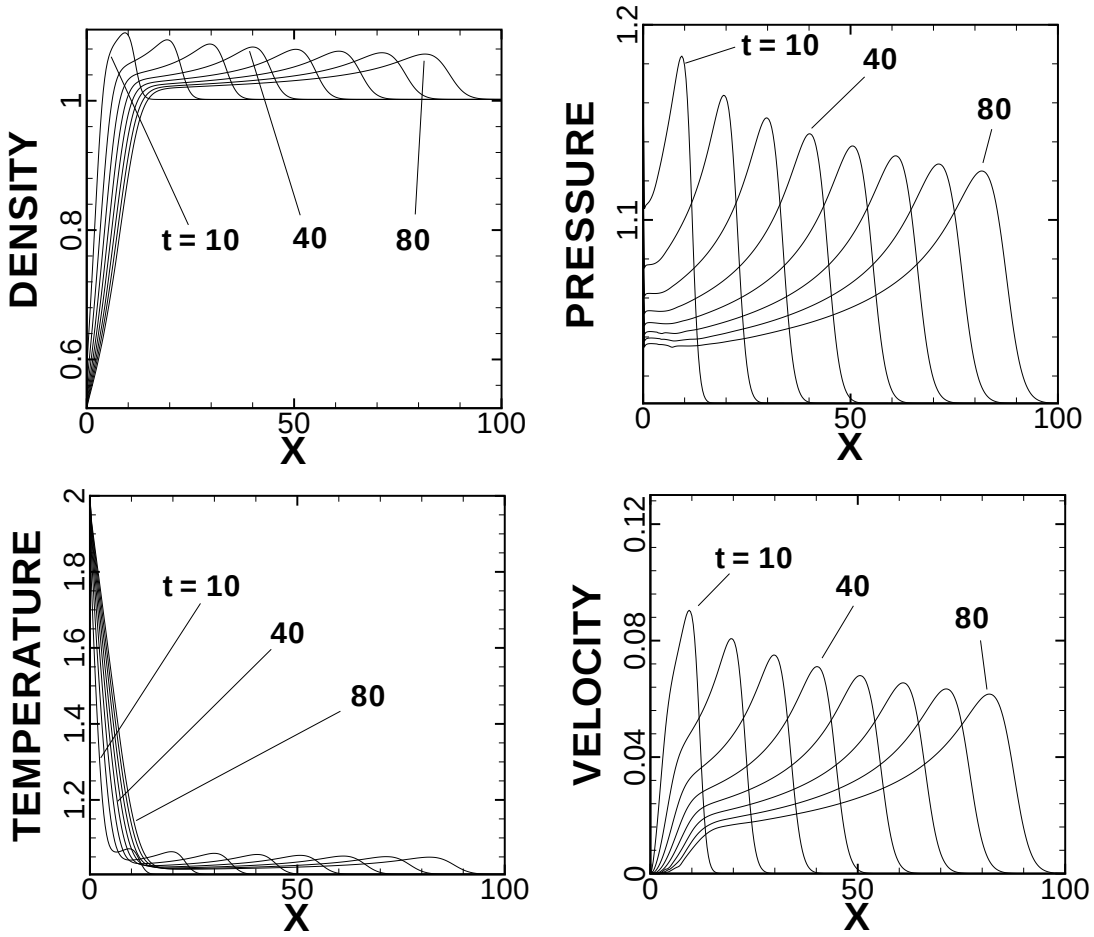

Figure 14: The time variation of density, temperature, velocity and pressure.

if such technical issues can be resolved by the Soroban grid and the number of grids in both coordinate space and velocity space could be reduced, however, there would be still some challenging issues. For example, physical modeling of real boundary condition is not yet established since the boundary condition in molecular level is unknown.

References

[1] Y. Sone, T. Ohwada and K. Aoki, Temperature jump and Knudsen layer in a rarefied gas over a plane wall: Numerical analysis of the linearized Boltzmann equation for hard-sphere molecules, Phys. Fluids A, 1 (1988), 363-370.

[2] C. K. Chu, Kinetic-theoretic description of the formation of shock wave, Phys. Fluids, 8 (1965), 12-22.

[3] G. A. Bird, The velocity distribution function within a shock wave, J. Fluid Mech., 30 (1967), 479-487.
[4] Y. Sone, Kinetic theory analysis of linearized Rayleigh problem, J. Phys. Soc. Jpn., 19 (1964), 1463-1473.
[5] J. Denavit, Numerical simulation of plasmas with periodic smoothing in phase space, J. Comput. Phys., 9 (1972), 75-98.
[6] G. A. Bird, Approach to translational equilibrium in a rigid sphere gas, Phys. Fluids, 6 (1963), 1518-1519.
[7] T. Ohwada, Structure of normal shock waves: Direct numerical analysis of the Boltzmann equation for hard-sphere molecules, Phys. Fluids A, 5 (1993), 217-234.
[8] H. Takewaki, A. Nishiguchi and T. Yabe, The cubic-interpolated pseudo-particle (CIP) method for solving hyperbolic-type equations, J. Comput. Phys., 61 (1985), 261-268.
[9] T. Yabe and T. Aoki, A universal solver for hyperbolic equations by cubic-polynomial interpolation, Comput. Phys. Commun., 66 (1991), 219-232.
[10] T. Yabe, T. Ishikawa, P. Y.Wang, T. Aoki, Y. Kadota and F. Ikeda, A universal solver for hyperbolic equations by cubic-polynomial interpolation II. Two- and three- dimensional solvers, Comput. Phys. Commun., 66 (1991), 233-242.
[11] T. Utsumi, T. Kunugi and T. Aoki, Stability and accuracy of the cubic interpolated propagation scheme, Comput. Phys. Commun., 101 (1996), 9-20.
[12] K. Takizawa, T. Yabe, M. Chino, T. Kawai, K. Wataji, H. Hoshino and T. Watanabe, Simulation and experiment on swimming fish and skimmer by CIP method, Comput. Struct., 83 (2005), 397-408.
[13] T. Kudoh, R. Matsumoto and K. Shibata, Numerical MHD simulation of astrophysical problems by using CIP-MOCCT method, CFD Journal, 8 (1999), 56-68.
[14] T. Yabe, F. Xiao and T. Utsumi, The constrained interpolation profile method for multiphase analysis, J. Comput. Phys., 169 (2001), 556-593.
[15] T. Nakamura and T. Yabe, Cubic interpolated propagation scheme for solving the hyperdimensional Vlasov-Poisson equation in phase space, Comput. Phys. Commun., 120 (1999), 122-154.
[16] Y. Kondoh, T. Yabe, J. Maehara, T. Nakamura and Y. Ogata, Microscopic and macroscopic simulations for femtosecond-laser-matter interaction by cubic-interpolated propagation method, Phy. Rev. E., 68 (2003), 066408-1-9.
[17] T. Yabe, H. Mizoe, K. Takizawa, H. Moriki, H.-N. Im and Y. Ogata, Higher-order schemes with CIP method and adaptive Soroban grid towards mesh-free scheme, J. Comput. Phys., 194 (2004), 57-77.
[18] A. Nishiguchi and T. Yabe, Second order fluid particle scheme, J. Comput. Phys., 52 (1983), 390-413.
[19] Y. Ogata, T. Yabe and K. Odagaki, An accurate numerical scheme for Maxwell equation with CIP-method of characteristics, Commun. Comput. Phys., 1 (2006), 311-335.
[20] P. L. Bhatnagar, E. P. Gross and M. Krook, A model for collision processes in gases. I. Small amplitude processes in charged and neutral one-component systems, Phys. Rev., 94 (1954), 511-525.
[21] H. Takewaki and T. Yabe, Cubic-interpolated pseudo-particle (CIP) method applications to nonlinear or multi-dimensional problems, J. Comput. Phys., 70 (1987), 355-372.
[22] T. Aoki, Multi-dimensional advection of CIP (cubic-interpolated propagation) scheme, CFD Journal, 4 (1995), 279-291.
[23] L. Desvillettes and S. Mischler, About the splitting algorithm for Boltzmann and B.G.K equa-

tions, Math. Mod. Meth. Appl. Sci., 6 (1996), 1079-1101.
[24] W. Cao, W. Huang and R. D. Russell, A study of monitor functions for two-dimensional adaptive mesh generation, SIAM J. Sci. Comput., 20(6) (1994), 1978-1994.
[25] H. Tang and T. Tang, Adaptive mesh methods for one- and two-dimensional hyperbolic conservation laws, SIAM J. Numer. Anal., 41 (2003), 487-515.
[26] K. Lipnikov and M. Shashkov, The error-minimization-based strategy for moving mesh methods, Commun. Comput. Phys., 1 (2006), 526-546.
[27] H.-Z. Tang, T. Tang and P.-W. Zhang, An adaptive mesh redistribution method for nonlinear Hamilton-Jacobi equations in two- and three dimensions, J. Comput. Phys., 188 (2003), 543-572.
[28] A. van Dam and P. A. Zegeling, A robust moving mesh finite volume method applied to 1D hyperbolic conservation laws from magnetohydrodynamics, J. Comput. Phys., 216 (2006), 526-546.
[29] G. Beckett, J. A. Mackenzie. and M. L. Robertson, An *r*-adaptive finite element method for the solution of the two-dimensional phase-field equations, Commun. Comput. Phys., 1 (2006), 805-826.
[30] K. W. Liang, P. Lin, M. Z. Ong and R. C. E. Tan, A splitting moving mesh method for reaction-diffusion equations of quenching type, J. Comput. Phys., 215 (2006), 757-777.
[31] C. Kim and A. Jameson, A robust and accurate LED-BGK solver on unstructured adaptive meshes, J. Comput. Phys., 143 (1998), 598-627.
[32] K. Takizawa, Numerical scheme for fluid flow including moving boundary and complex surface by Soroban grid CIP method, Ph.D thesis, Tokyo Institute of Technology, Japan, 2005.
[33] K. Takizawa1, T. Yabe, Y. Tsugawa, T. E. Tezduyar and H. Mizoe, Computation of free-surface flows and fluid-object interactions with the CIP method based on adaptive meshless Soroban grids, Comput. Mech., to be published.
[34] S. T. Zalesak, Fully multidimensional flux-corrected transport algorithm for fluids, J. Comput. Phys., 31 (1979), 335-362.
[35] L. H. Holway Jr, New statistical models for kinetic theory, methods of construction, Phys. Fluids, 9 (1966), 1658-1673.
[36] L. Mieussens, Discrete-velocity models and numerical schemes for the Boltzmann-BGK equation in plane and axisymmetric geometries, J. Comput. Phys., 162 (2000), 429-466.
[37] Z.-H. Li and H.-X. Zhang, Study on gas kinetic unified algorithm for flows from rarefied transition to continuum, J. Comput. Phys., 193 (2004), 708-738.
[38] E. F. Toro, Riemann Solvers and Numerical Methods for Fluid Dynamics, Springer-Verlag, Berlin, 1999.
[39] K. Aoki, Y. Sone, K. Nishino and H. Sugimoto, Numerical analysis of unsteady motion of a rarefied gas caused by sudden changes of wall temperature with special interest in the propagation of a discontinuity in the velocity distribution function, Rarefied Gas Dynamics, (1991), 222-231.
[40] Y. Sone, T. Ohwada and K. Aoki, Evaporation and condensation on a plane condensed phase: Numerical analysis of the linearized Boltzmann equation for hard-sphere molecules, Phys. Fluids A, 1 (1989), 1398-1405.